Polyhedron 30 (2011) 690–696

Contents lists available at ScienceDirect

Polyhedron

journal homepage: www.elsevier.com/locate/poly

# Solution structures of fluorescent Zn(II) complexes with bis(naphthyl amide)–EDTA

Hisila Santacruz *, Rosa Elena Navarro, Lorena Machi *, Rocío Sugich-Miranda, Motomichi Inoue

*Departamento de Investigación en Polímeros y Materiales, Universidad de Sonora, Hermosillo, Sonora 83000, Mexico*

ARTICLE INFO

*Article history:*
Received 18 October 2010
Accepted 1 December 2010
Available online 7 December 2010

*Keywords:*
Bichromophores
EDTA
Fluorescence
Naphthalene
NMR
Zn complexes

ABSTRACT

Two EDTA-based bichromophoric isomers form Zn(II) complexes that exhibit distinct fluorescent behaviors; the ligands are abbreviated as (edta1nap)$H_2$ and (edta2nap)$H_2$, each of which consists of an EDTA chain linked to two 1-naphthyl or 2-naphthyl groups. The coordination chemistry of these complexes was studied by UV–Vis, fluorescence and $^1$H NMR. The formation constants and the inherent emission intensities were determined by the pH dependence of the emission spectra; the species of the most intense emission is ML(OH) for L = (edta1nap)$^{2-}$, and ML for (edta2nap)$^{2-}$. The $^1$H NMR of Zn-(edta1nap)$^{2-}$ exhibits two sets of signals due to a slow exchange between two equivalent coordination geometries, whereas Zn-(edta2nap)$^{2-}$ undergoes a fast exchange to show a single set of NMR signals. The spin–lattice relaxation time $T_1$ determined for the isostructural Mn(II) complexes shows that the naphthyl proton closest to the metal ion is H(8) in the (edta1nap)$^{2-}$ complex, and H(3) in the (edta2nap)$^{2-}$ complex. The two ligands differ only in the substitution position of the naphthyl group, but this apparently small difference leads to the notable difference in structural, dynamic, and consequent emission-spectral properties of their metal complexes as a result of the steric and size effects of the aromatic rings.



## 1. Introduction

A bichromophore composed of two identical aromatic rings, such as naphthalene and pyrene, exhibits emission from an intramolecular excimer when the aromatic rings are linked by an appropriate chain. This type of emission is more sensitive to an environmental change than is emission from a monomeric (or isolated) hydrocarbon molecule [1–12]. When electron-donating atoms are integrated into the interlinking chain between fluorescent units, the resulting chelating bichromophore is expected to function as a highly sensitive fluorescent sensor toward specific metal ions, because any conformational change caused by metal coordination influences the excimer emission strongly [3–12]. The selection of appropriate chelating chain is the most crucial factor in the molecular design. From this viewpoint, we have synthesized ethylenediaminetetraacetic (EDTA) and diethylenetriaminepentaacetic (DTPA) derivatives in which both ends of a chelating chain are bound to naphthyl or pyrenyl groups through amide linkages [10–12]. Among them, EDTA-naphthyl derivatives, shown in Scheme 1 with the abbreviations, are capable of forming 1:1 complexes with Zn(II), and the excimer emission is sharply intensified upon complexation whereas the emission is unchanged or weakened upon complexation with other metal ions such as Cd(II) [10]. Thus, the two isometic bis(naphthyl amide)–EDTA ligands can sense Zn(II) specifically. It is noteworthy that these ligands show a significant difference in spectral changes upon complexation: for example, the band maximum of (edta1nap)$H_2$ is shifted to shorter wavelengths whereas that of (edta2nap)$H_2$ does not undergo any shift, although the excimer emissions of both derivatives are intensified in a similar manner. This spectral difference is supposed to be associated with the orientations of naphthyl groups and the consequent stacking in the Zn(II) complexes in solution. These conceivable structural effects on fluorescence, as well as the specific sensing capability of the ligands toward Zn, have prompted us to study the structures of the Zn(II) complexes in solution. In this work, we report (1) the metal-chelate species formed in solution and their formation constants determined by the pH dependence of the excimer emissions and (2) the structural and dynamic properties determined by $^1$H NMR. As supporting experiments, $^1$H NMR relaxation time $T_1$ has been measured on the isostructural paramagnetic Mn(II) complexes.

## 2. Experimental

The bichromophoric ligands were synthesized by the methods reported previously, and characterized by $^1$H NMR [10].

Absorption spectra were recorded on a Perkin–Elmer Lambda 20 spectrophotometer. Fluorescence spectra were obtained with

* Corresponding authors.
*E-mail addresses:* hisila@polimeros.uson.mx (H. Santacruz), lmachi@polimeros.uson.mx (L. Machi).

0277-5387/$ - see front matter © 2010 Elsevier Ltd. All rights reserved.
doi:10.1016/j.poly.2010.12.002

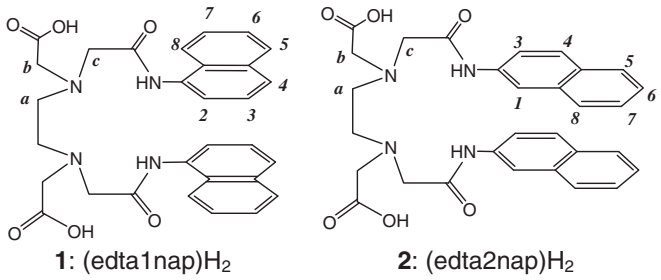


**Scheme 1.** Bis(naphthyl amide)–EDTA derivatives and their abbreviations.

a Perkin–Elmer LS-50B Luminescence Spectrometer. In the studies of coordination of (edta1nap)$H_2$ and (edta2nap)$H_2$ with $Zn^{2+}$, the absorption and emission spectra of ligand solutions (3 mL, $1 \times 10^{-5}$ M) were observed at pH 10 ($NaHCO_3$/NaOH buffer) and 8.5 (Tris buffer), while aliquots (5 μL each) of a $Zn^{2+}$ solution ($6 \times 10^{-4}$ M) were added with a calibrated micropipette. Sample solutions for studying the pH dependence of the emission spectra were prepared as follows. A stock solution was prepared which contained an appropriate ligand and $Zn^{2+}$ ion in the mole ratio $[M]_t/[L]_t = 0.95–1$ in 0.01 M NaCl; the ligand was in slight excess to suppress the precipitation of metal hydroxide. To a half of the solution, 0.001 M NaOH was added so that the pH was a desired highest value, and the pH of the other half was adjusted to a lowest value with 0.001 M HCl. By mixing the two solutions in appropriate ratios, sample solutions of different pH values were prepared while the sample concentration and ionic strength were kept constant. Emission intensities of the Zn complexes were normalized against the most intense band of the corresponding free ligands. $^1$H NMR spectra were obtained with a Bruker Avance 400 NMR spectrometer at a probe temperature of 25 °C with DSS as the internal standard. Relaxation time $T_1$ was determined by the $180° - \tau - 90°$ pulse sequence technique with a pulse width of 8.75 μs for 90° pulse.

## 3. Results and discussion

### 3.1. Fluorescence spectra and formation constants of Zn(II) complexes

Our previous studies of the emission spectra indicated the formation of a 1:1 complex between each ligand and $Zn^{2+}$ [10]. The compositions have been confirmed further by absorption spectroscopy as follows. Both ligands exhibit a broad band at 280 nm and a shoulder at 290 nm (Fig. 1). The addition of $Zn^{2+}$ to $(edta1nap)^{2-}$ leads to hypochromic and bathochromic changes of the main band accompanied by an isosbestic point at 295 nm (Fig. 1). On the other hand, the addition of $Zn^{2+}$ to $(edta2nap)^{2-}$ weakens the main band and strengthens a secondary band at 330 nm; both bands do not undergo a shift, and an isosbestic point appears at 305 nm. In both metal–ligand systems, the absorptivity at a given wavelength changes linearly up to the ratio of the total concentrations $[Zn]_t/[L]_t = 1$; above this ratio the absorptivity is unchanged (insets of Fig. 1). These spectral behaviors support the formation of 1:1 complexes; this stoichiometry has been confirmed by Job's plot as well.

The emission spectrum of the Zn-$(edta1nap)^{2-}$ complex exhibits a strong excimer band around 450 nm and a weak band around 370 nm; the former band undergoes a blue shift with increasing pH and the intensity is changed sensitively to pH (Fig. 2). For the $(edta2nap)^{2-}$ complex, only the excimer band is observed around 420 nm; the intensity is varied with pH without showing a change in the band shape (Fig. 2). The intensity $I_E$ of the excimer band at a given wavelength is plotted against pH

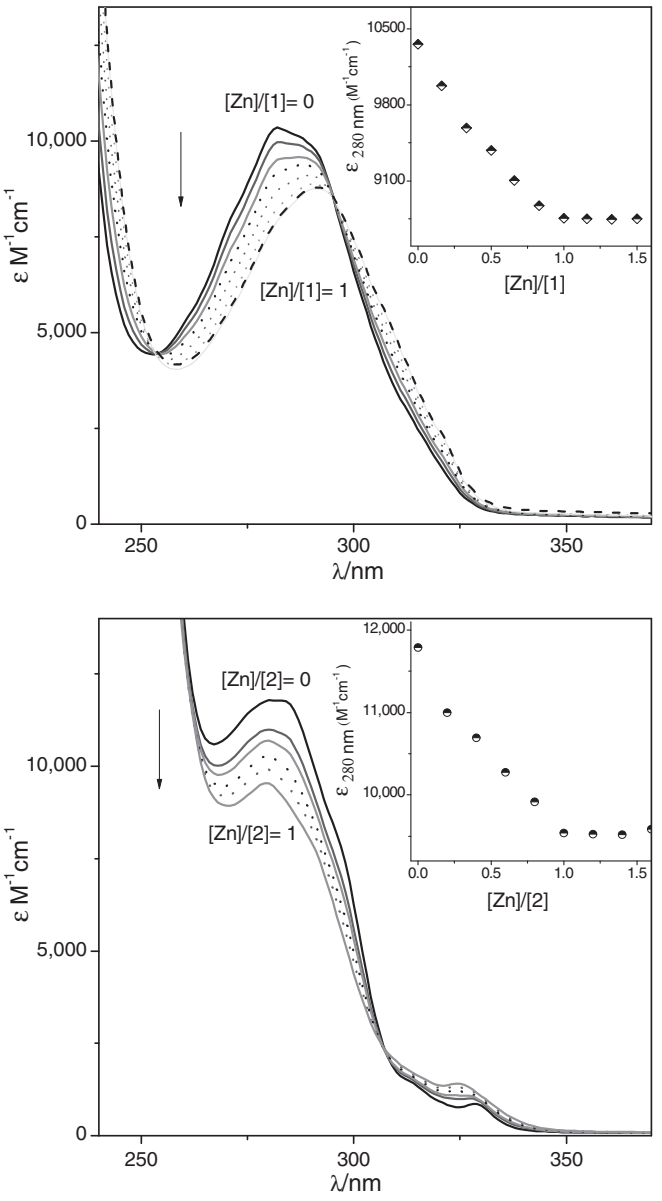


**Fig. 1.** Electronic absorption spectra of (**1**) (edta1nap)$H_2$ (top) and (**2**) (edta2nap)$H_2$ (bottom) in the presence of $Zn^{2+}$ in different mole ratios $[Zn]_t/[L]_t$ from 0 to 1; $[L]_t$, $1 \times 10^{-5}$ M, pH, 10 (0.1 M NaOH/0.05 M $NaHCO_3$ buffer). Inset: molar absorptivity at 280 nm as a function of $[Zn]_t/[L]_t$.

for the $(edta1nap)^{2-}$ and $(edta2nap)^{2-}$ complexes in Figs. 3 and 4, respectively. Since each ligand forms a 1:1 metal complex with Zn(II), the observed spectral changes suggest that the main species ML is accompanied by secondary species such as $MLH_m$ and $MLH_{-n}$ (or $ML(OH)_n$).

The emission intensity is given by an average over coexisting species at a certain pH value, as follows.

$$I_E(pH) = \left\{ \sum_x I_E(MLH_x) \cdot [MLH_x] + \sum_l I_E(LH_l) \cdot [LH_l] \right\} / [L]_t \qquad (1)$$

Here, $[MLH_x]$ is molar concentration of $MLH_x$, $I_E(MLH_x)$ is the emission intensity inherent in species in the parenthesis, integer $x$ ranges from $m$ to $-n$, and $[L]_t$ is the total concentration of the ligand. The concentration of each species can be formulated by combining formation constants, protonation constants and mass balances, which are defined, respectively, as follows.

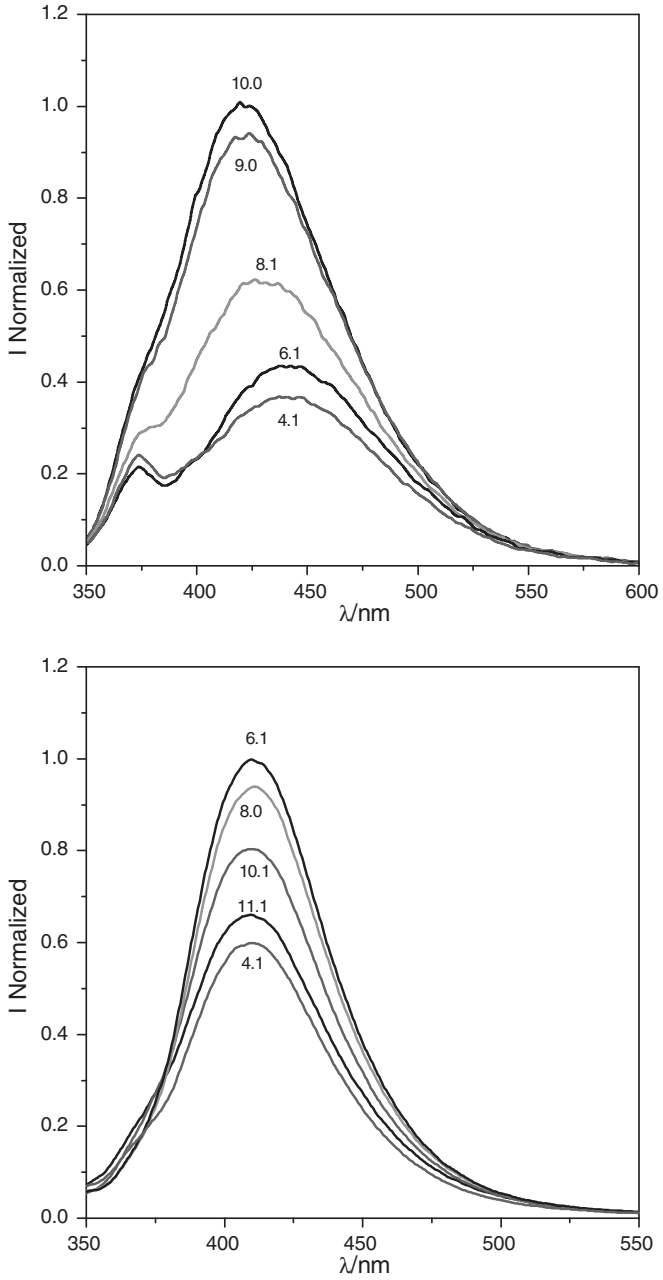


**Fig. 2.** Fluorescence emission spectra of (top) Zn-(edta1nap)$^{2-}$ and (bottom) Zn-(edta2nap)$^{2-}$ at different pH values: $[L]_t$, $1 \times 10^{-5}$ M; $[Zn]_t/[L]_t$, 0.95; ionic strength, 0.01 M (NaCl); excitation wavelength, 330 nm for Zn-(edta1nap)$^{2-}$ and 280 nm for Zn-(edta2nap)$^{2-}$; $T$, 25 °C.

$$K_{ML} = [ML]/[M][L] \quad (2)$$

$$K_{MLHm} = [MLH_m]/[MLH_{m-1}][H] \quad (3)$$

$$K_{MLH-n} = [MLH_{-n}][H]/[MLH_{-n+1}] \quad (4)$$

$$K_{LHl} = [LH_l]/[LH_{l-1}][H] \quad (5)$$

$$[M]_t = [M] + \sum_x [MLH_x] \quad (6)$$

$$[L]_t = \sum_x [MLH_x] + \sum_l [LH_l] \quad (7)$$

If the protonation constants, $K_{LHl}$, and the inherent intensities, $I_E(LH_l)$, of the ligand are known, the formation constants of the metal complexes can be determined by searching for the set of parameters, $K_{MLHx}$ and $I_E(MLH_x)$, that gives the best fit of Eq. (1) to the observed $I_E$ versus pH plot by means of non-linear least-squares calculations [13]. The parameters of the ligands have been determined from $I_E$ versus pH plots observed for the free ligands: log $K_{LH}$ = 6.77 and log $K_{LH2}$ = 3.85 for (edta1nap)$H_2$; log $K_{LH}$ = 7.20 and log $K_{LH2}$ = 3.11 for (edta2nap)$H_2$. In least-squares calculation processes, the species formed in each metal–ligand system have been detected by inspecting fitness between the shapes of the

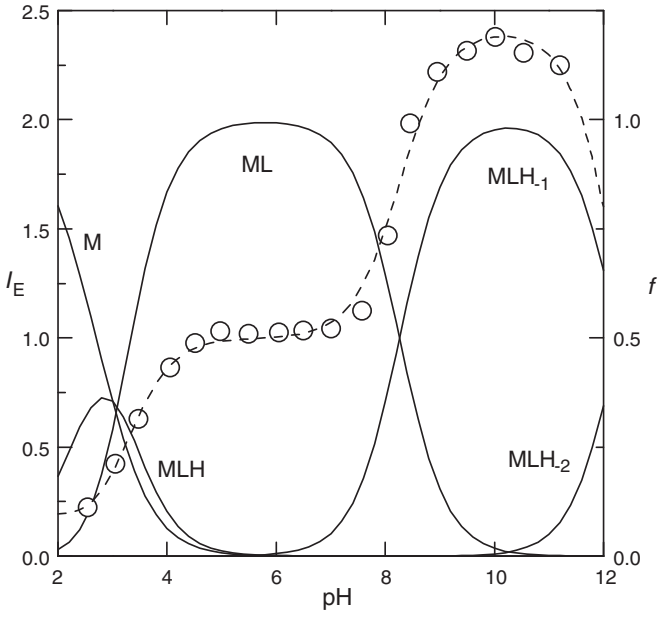


**Fig. 3.** Intensity of excimer emission $I_E$ observed at 420 nm for Zn-(edta1nap)$^{2-}$ at different pH values: $[Zn]_t$, $0.95 \times 10^{-5}$ M; $[L]_t$, $1.0 \times 10^{-5}$ M; ionic strength, 0.01 M (NaCl); $T$, 25 °C. The emission intensity is referenced to that of the most intense band of the free ligand. The dotted line shows the best fit obtained by non-linear least-squares fitting. The solid lines present the mol fractions $f$ (against $[Zn]_t$) of the metal complex species.

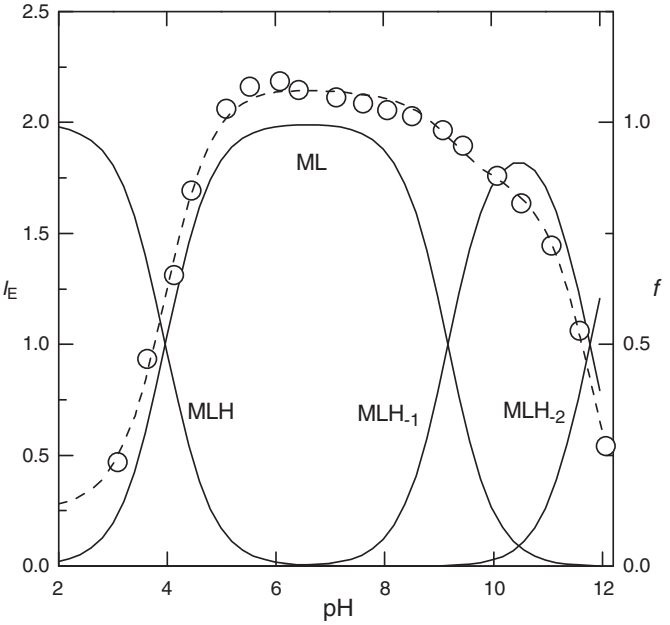


**Fig. 4.** Intensity of excimer emission $I_E$ observed at 404 nm for Zn-(edta2nap)$^{2-}$ at different pH values: $[Zn]_t$, $0.95 \times 10^{-5}$ M; $[L]_t$, $1.0 \times 10^{-5}$ M; ionic strength, 0.01 M (NaCl); $T$, 25 °C. The emission intensity is referenced to that of the most intense band of the free ligand. The dotted line shows the best fit obtained by non-linear least-squares fitting. The solid lines present the mol fractions $f$ (against $[Zn]_t$) of the metal complex species.

**Table 1**
Logarithmic formation constants log $K_{MLHx}$ of Zn complexes with (edta1nap)$H_2$ and (edta2nap)$H_2$, and excimer emission intensities $I_E$ inherent in species $MLH_x$ ($x$ = 0, 1, −1 or −2) in 0.01 M NaCl at 25 °C: $K_{ML}$ = [ML]/[M][L], $K_{MLH}$ = [MLH]/[ML][H], $K_{MLH-1}$ = [$MLH_{-1}$][H]/[ML] and $K_{MLH-2}$ = [$MLH_{-2}$][H]/[$MLH_{-1}$]; $I_E$ is referenced to the highest intensity of the corresponding free ligand.

| | Log K[a] | | | | $I_E$ | | | |
|---|---|---|---|---|---|---|---|---|
| | ML | MLH | $MLH_{-1}$ | $MLH_{-2}$ | MLH | ML | $MLH_{-1}$ | $MLH_{-2}$ |
| $(edta1nap)^{2-}$ | 10.1 | 3.1 | −8.3 | −12.3 | 0 | 1.0 | 2.5 | 0 |
| $(edta2nap)^{2-}$ | 10.7 | 4.0 | −9.1 | −11.7 | 0.3 | 2.2 | 1.8 | 0 |

[a] The estimated uncertainties of log $K_{MLHx}$ are 5% for the main species and 10% for the secondary species.

observed and calculated curves and by minimizing the deviation defined as $[\Sigma(I_{E,obs} - I_{E,cal})^2/(N-k)]^{1/2}$ where $N$ is the number of data points and $k$ is the number of parameters.

Table 1 presents the detected species, their formation constants and inherent emission intensities. The species distributions calculated from the formation constants are well correlated to the changes in the emission intensity with pH, as shown in Figs. 3 and 4. The metal complexation occurs even at pH as low as ∼3 to yield MLH species, unlike polyamines modified with naphthyl groups; the latter ligands undergo complexation above pH 6 [3,14–17]. The complexation of the EDTA-naphthyl derivatives in a wider pH range is attributable to the presence of carboxylate groups [10,11]. The neutral species ML is converted to the hydroxides $ML(OH)_n$ at high pH. The formation constants of the Zn(II) complexes of the 1-naphthyl and 2-naphthyl derivatives are of the same order of magnitude. On the other hand, the emission intensities show a notable difference: the species that exhibits the most intense emission is ML(OH) for L = $(edta1nap)^{2-}$, and ML for $(edta2nap)^{2-}$. The two ligands have the same coordination sites, and differ only in the substitution position of the fluorescent unit. This apparently small difference leads to the notable difference in the absorption and emission-spectral properties, which are supposed to be closely associated with the stacking mode of naphthyl groups.

### 3.2. $^1$H NMR of Zn complexes

In order to corroborate the possible structural difference between the Zn(II) complexes, $^1$H NMR studies have been carried out. Fig. 5 shows the $^1$H NMR spectra observed for the Zn(II) complexes at pD 9 and 298 K, along with spectra of the uncoordinated ligands for comparison. At this pD, the ligands form $L^{2-}$ species and the major species of the Zn(II) complexes are $[ZnL]^0$. The signals of the Zn(II) complexes can be assigned by comparison with those of the corresponding uncoordinated ligands and by examination of the coupling patterns in two-dimensional correlation spectra (COSY). Every set of equivalent protons in the free ligands exhibits only a single signal as a result of a fast exchange. Such equivalencies are lost in the Zn(II) complexes due to a rigidity of the metal chelate rings. EDTA-based tetraazamacrocycles that integrate two amide groups in the ring system and bear two pendant carboxyl groups have been reported to commonly form distorted octahedral metal complexes consisting of two ethylenediamine nitrogens, two carboxylate oxygens and an amide oxygen together with a water oxygen [18–20]. A similar coordination is supposed to be formed in Zn-$(edtanap)^{2-}$ complexes, as illustrated in Scheme 2A. This structure, in which halves in the molecule are unequal, is converted reversibly to an equivalent structure at a certain rate of conversion.

The (edta2nap)$H_2$ complex exhibits an ABXY pattern of the ethylenediamine chain, an AB pattern of $CH_2$(b) bound to carboxyl, a singlet of $CH_2$(c) adjacent to amide groups, and a multiplet of the aromatic group. In contrast, two sets of such patterns are observed for the (edta1nap)$H_2$ complex; the integrated intensities of the corresponding signals are exactly identical. Essentially the same spectrum is observed at a higher pD (∼10) at which the ML(OH) species is formed. These spectral behaviors of the (edta1nap)$H_2$ complex

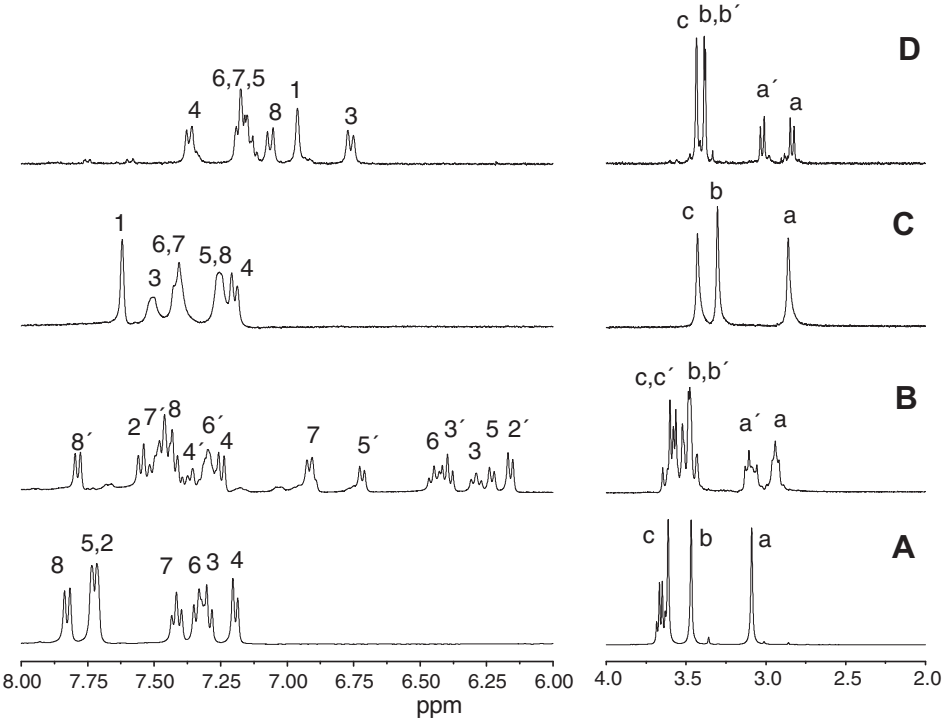


**Fig. 5.** $^1$H NMR spectra of (A) (edta1nap)$H_2$, (B) its Zn complex, (C) (edta2nap)$H_2$ and (D) its Zn complex in $D_2O$ at pD 9. For labeling of protons, see Scheme 1. The quartets around 3.7 ppm in spectra A and B are due to ethanol involved in its adduct of (edta1nap)$H_2$.

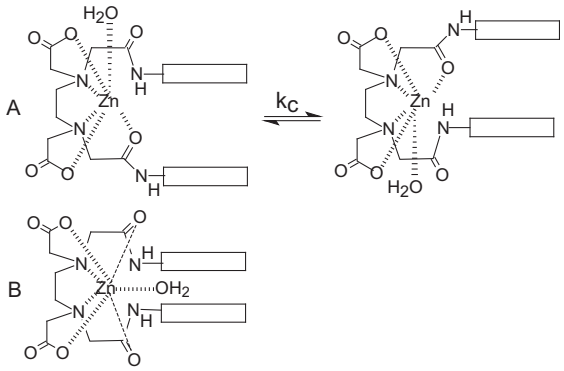


**Scheme 2.** (A) Coordination mode and interconversion between equivalent geometries in the Zn complexes of bis(naphthyl amide)–EDTA, and (B) a time-averaged structure; rectangles show naphthalene rings. In [Zn(edta1nap)($H_2O$)], the rate of interconversion is so low that $^1$H NMR distinguishes between two conformations. In [Zn(edta2nap)($H_2O$)], the interconversion is so fast that the time-averaged structure B is recognized by $^1$H NMR; amide C=O oxygen atoms occupy the second coordination sphere.

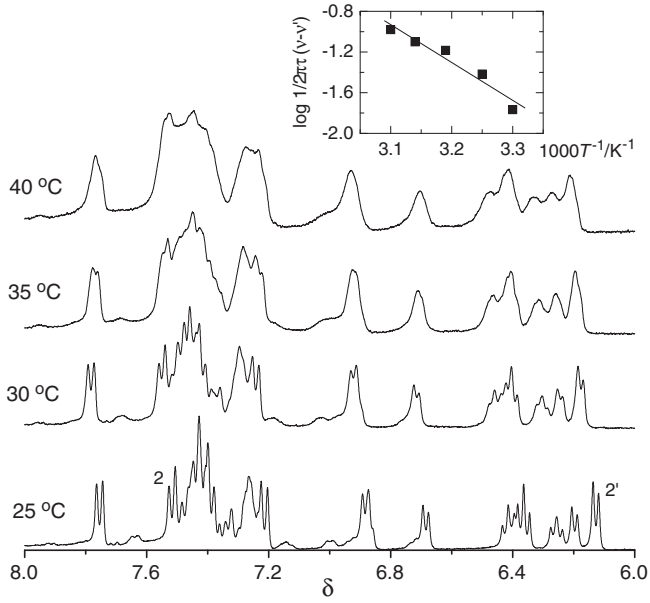


**Fig. 6.** Temperature dependence of aromatic proton NMR signals of Zn(edta1nap) at pD = 9. The inset shows a plot of log $1/2\pi\tau(\nu-\nu')$ versus $1/T$ for a pair of protons 2 and 2′; the straight line gives 70 kJ mol$^{-1}$ for the barrier height for interconversion shown in Scheme 2A.

indicate that (1) the two sets of signals are due to the inequality of the halves in the ZnL molecule rather than to the coexistence of other species and (2) the coordination modes in ZnL and ZnL(OH) are essentially identical and indistinguishable by NMR. In the [ZnL(OH)] species, an OH group is simply substituted for a $H_2O$ molecule in [ZnL($H_2O$)] without influencing the coordination of the donor atoms of the ligand.

The observation of two sets of signals for [Zn(edta1nap)($H_2O$)] shows that the rate of the interconversion in Scheme 2A is much lower than the $^1$H NMR observation frequency. This slow exchange has been confirmed by variable-temperature NMR spectra, in which the elevation of temperature broadens signals and makes a pair of peaks closer toward each other (Fig. 6). The rate constant $k_c$ for the conversion in Scheme 2A is expressed by:

$$k_c = k_0 \exp(-E/RT) \tag{8}$$

Here, $k_0$ is the frequency factor and $E$ is the potential barrier for the interconversion. This equation can be modified as [21]:

$$\log_{10} 1/2\pi\tau(\nu-\nu') = \log_{10} k_0/\pi(\nu-\nu') - E/2.3\mathrm{RT} \tag{9}$$

Here, $\tau$ is the mean lifetime of the states, and $\nu-\nu'$ is the difference between the resonance frequencies of a pair of protons. The value of $\tau(\nu-\nu')$ can be determined from the ratio of peak separations on the basis of the shape function when $|\nu-\nu'|$ is very large compared with the line width [21]. Protons 2 and 2′ are selected for this calculation, because the signals are well separated from each other and less interfered with neighboring signals. A log $1/2\pi\tau(\nu-\nu')$ versus $1/T$ plot shown in the inset of Fig. 6 yields $E$ = 70 (±10) kJ mol$^{-1}$ and $k_0 \sim 7 \times 10^{13}$ Hz.

[Zn(edta2nap)($H_2O$)] exhibits a single set of spectrum, which indicates the equivalence of the halves in the molecule. The coordination of an amide oxygen is supposed to be weak, because the absorption and emission bands of (edta2nap)$H_2$ are not shifted by metal coordination, in contrast to the clear shift of the peak maximum of [Zn(edta1nap)($H_2O$)] (Fig. 1). As a result of the weak coordination of amide oxygen in Zn-(edta2nap)$^{2-}$, the structural interconversion in Scheme 2A is fast compared with the $^1$H NMR observation time scale so that NMR recognizes a time-averaged structure illustrated in Scheme 2B in which two amide groups are equivalent. The fast exchange is supported by the fact that a singlet is observed for $CH_2$(c) bonded to amide in [Zn(edta2nap)($H_2O$)] whereas the corresponding proton signal of [Zn(edta1nap)($H_2O$)] is composed of two doublets.

The metal coordination results in a decrease in the $\delta$ values of the naphthyl protons (Table 2). These changes in $\delta$, $\Delta\delta$, of [Zn(edta2nap)($H_2O$)] are ascribable to the ring current effect from the other naphthyl ring in the same molecule, because the amide oxygen atoms are loosely bound to the metal ion. The chemical shift $\delta_{rc}$ caused by a naphthyl ring at a nearby resonant proton is calculated by the sum of the dipole fields induced by two component hexagons as described in Appendix [21]. The calculated $\delta_{rc}$ values shown in Table A1 (in Appendix) indicate that the ring current effect is large enough to result in the observed changes in $\delta$. Upon formation of [Zn(edta2nap)($H_2O$)], two naphthalene rings move closer toward each other at CH(1) and CH(3), because they show the largest change in $\delta$; the closest contacts are predicted to be

**Table 2**
Chemical shifts $\delta$ (ppm) of uncoordinated ligands, (edta1nap)$H_2$ and (edta2nap)$H_2$, and their Zn(II) complexes, and the differences between the shifts, $\Delta\delta = \delta(\mathrm{ZnL}) - \delta(\mathrm{L})$, in $D_2O$ at $T$, 25 °C and pD, 9.0.

| Proton | (edta1nap)$H_2$ | | | (edta2nap)$H_2$ | | |
|---|---|---|---|---|---|---|
| | $\delta$(L) | $\delta$(ZnL) | $\Delta\delta$ | $\delta$(L) | $\delta$(ZnL) | $\Delta\delta$ |
| a | 3.09 | 2.80 | −0.29 | 2.90 | 2.85 | −0.05 |
| a′ | | 2.90 | −0.19 | | 3.04 | 0.14 |
| b | 3.48 | 3.35 | −0.13 | 3.32 | 3.41 | 0.09 |
| b′ | | 3.28 | −0.20 | | 3.40 | 0.08 |
| c | 3.63 | 3.43 | −0.20 | 3.47 | 3.46 | −0.01 |
| c′ | | 3.48 | −0.15 | | | |
| 1 | | | | 7.63 | 6.98 | −0.65 |
| 2 | 7.72 | 7.54 | −0.18 | | | |
| 2′ | | 6.15 | −1.57 | | | |
| 3 | 7.34 | 6.29 | −1.05 | 7.57 | 6.79 | −0.78 |
| 3′ | | 6.39 | −0.95 | | | |
| 4 | 7.23 | 7.24 | 0.01 | 7.22 | 7.09 | −0.13 |
| 4′ | | 7.36 | 0.13 | | | |
| 5 | 7.72 | 6.22 | −1.50 | 7.32 | 7.14 | −0.18 |
| 5′ | | 6.71 | −1.01 | | | |
| 6 | 7.37 | 6.49 | −0.88 | 7.47 | 7.19 | −0.28 |
| 6′ | | 7.29 | −0.08 | | | |
| 7 | 7.45 | 6.91 | −0.54 | 7.47 | 7.19 | −0.28 |
| 7′ | | 7.49 | 0.04 | | | |
| 8 | 7.82 | 7.44 | −0.38 | 7.32 | 7.17 | −0.15 |
| 8′ | | 7.78 | −0.04 | | | |

in the range 3.5–4.0 Å, or slightly longer than the van der Waals contact, 3.4 Å, of aromatic carbon. This closer contact is responsible for the higher efficiency of excimer formation in the metal complex [10]. For [Zn(edta1nap)($H_2O$)], two naphthyl groups show irregular changes in $\delta$; the largest changes are observed for H(5) of one ring and for H(2′) of the other. Small positive changes in $\delta$ of H(4), H(4′) and H(7′) show that these protons are slipped further from the center of the other ring upon complexation, and are located in the positive $\delta_{rc}$ region with the large angle from the normal to the center of the counter ring. These observations support that the naphthyl groups are not equivalent in their stack as a result of the slow structural exchange shown in Scheme 2A.

### 3.3. $^1$H NMR relaxation times of Mn(II) complexes

The $^1$H NMR shows that the orientations of naphthyl groups are responsible for the emission properties distinct between the Zn(II) complexes. As supporting data, $^1$H NMR spin–lattice relaxation time $T_1$ has been determined for the corresponding Mn(II) complexes which are supposed to be isostructural with the Zn(II) complexes [18,20,22,23]. The $T_1$ of every proton was shortened with the increase of the concentration of coexisting paramagnetic $Mn^{2+}$ ion at a constant concentration of a ligand, as shown in Fig. 7 in which the inverse of the relaxation time, $1/T_1$, is plotted for selected protons against the ratio of the total concentrations of Mn and ligand, $[Mn]_t/[L]_t$. Since all Mn(II) ions form the complexes with the ligand molecules under the experimental condition $[Mn]_t \ll [L]_t$, the inverse of $T_1$ of proton $n$ is expressed by a linear function of $[Mn]_t$ as follows [24,25].

$$1/T_{1,n} = (1/T_{1ML,n})[Mn]_t/[L]_t + 1/T_{1L,n} \quad (10)$$

This equation well interprets the observed $1/T_1$ data (Fig. 7), and the intercept determined by linear fitting for every proton agrees with the corresponding $1/T_1$ observed at $[Mn]_t = 0$ within the standard deviation. This observation supports the validity of Eq. (10). The $1/T_{1ML}$ values are determined as listed in Table 3.

The paramagnetic effect on $^1$H NMR relaxation originates from the dipolar term and the Fermi contact term. For $Mn^{2+}$ complexes, the latter term is negligible so that $T_{1ML}$ is defined only by the dipolar term, which is given by [24]:

$$1/T_{1ML,n} = (4/3)S(S+1)(g_e^2 g_n^2 \mu_e^2 \mu_n^2/\hbar^2)\tau_c r_n^{-6} \quad (11)$$

Here, apart from the obvious notations, $\tau_c$ is the correlation time of dipolar interaction, and $r_n$ is the distance between the resonant proton $n$ and the central metal ion in a complex molecule. The practically identical $1/T_{1ML}$ values of H(a) in ethylenediamine unit of two metal complexes suggest similarity in the dynamic and structural properties of the metal–ethylenediamine chelate rings. In contrast, H(c) adjacent to amide group has different $1/T_{1ML}$ values, supporting that the metal complexes involve different coordination modes of the amide oxygen. A clear distinction in the $1/T_{1ML}$ is also found for naphthyl protons. For example, H(8) shows the largest $1/T_{1ML}$ among aromatic protons in Mn(edta1nap), whereas the $1/T_{1ML}$ of H(3) is largest in Mn(edta2nap). Since the internal motion of a naphthyl ring governs the correlation times of the protons attached to the ring, the aromatic protons neighboring the carbon atom bound to amide group are supposed to have $\tau_c$ of the same order of magnitude. When the $1/T_{1ML}$ values of CH(2) and CH(8) on either side of C(1) in Mn(edta1nap) are compared, $1/T_{1ML}$ is correlated to $r^{-6}$. Therefore, the larger $1/T_{1ML}$ value of CH(8) indicates that this proton is in a closer proximity to the metal ion than is CH(2). Similarly, in Mn(edta2nap), CH(3) is closer to the central metal than is CH(1). Thus, the $T_1$ measurements have taken a view of the orientation of naphthalene rings in the metal complexes.

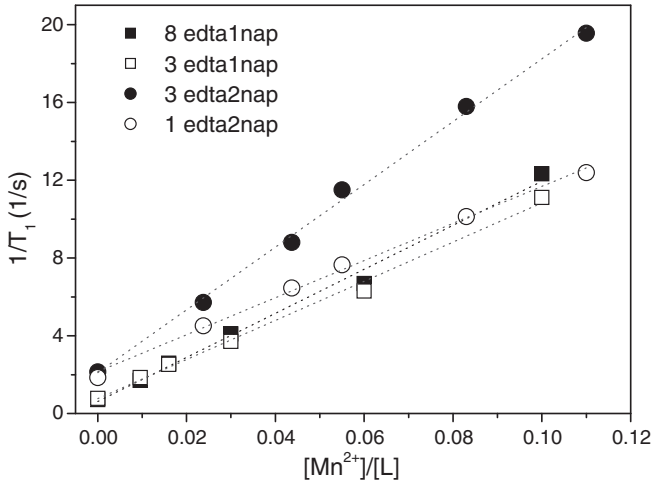


**Fig. 7.** Inverse relaxation time $1/T_1$ versus $[Mn]_t/[L]_t$ plots of selected protons of (edta1nap)$H_2$ and (edta2nap)$H_2$.

**Table 3**
Inverse $^1$H NMR relaxation time, $1/T_{1ML}$ ($s^{-1}$), of (**1**) Mn(II)-(edta1nap)$H_2$ and (**2**) Mn(II)-(edta2nap)$H_2$, and $1/T_{1L}$ ($s^{-1}$) at $[Mn]_t \to 0$; pD, 7.7; $T$, 25 °C.

| Proton | $1/T_{1ML}$ | | $1/T_{1L}$ | |
|---|---|---|---|---|
| | **1** | **2** | **1** | **2** |
| H(a) | 57 | 61 | 3.68 | 3.84 |
| H(b) | 92 | 80 | 2.73 | 3.33 |
| H(c) | 86 | 108 | 2.97 | 3.94 |
| H(1) or H(2) | 89 | 95 | 0.72 | 1.85 |
| H(3) | 113 | 161 | 0.78 | 2.14 |
| H(4) | 84 | 85 | 0.63 | 2.30 |
| H(5) | 89 | 103 | 0.72 | 2.11 |
| H(6) | 81 | 117 | 0.82 | 1.98 |
| H(7) | 106 | 117 | 0.76 | 1.98 |
| H(8) | 113 | 103 | 0.72 | 2.11 |

### 3.4. Structure and fluorescence

The structural features concluded by NMR for the Zn(II) complexes are summarized as follows: (1) the naphthyl rings are stacked closer upon complexation to enhance the excimer emission; (2) in [Zn(edta1nap)($H_2O$)], only one amide oxygen atom is bonded to the central metal, and this coordination, together with the steric and size effects of naphthyl groups, results in a slow interconversion between two equivalent coordination geometries; (3) in [Zn(edta2nap)($H_2O$)], amide oxygen atoms coordinate the central metal so weakly as to facilitate the geometrical interconversion, and two naphthyl groups are equivalent in the NMR time scale. The spin–lattice relaxation time determined for the Mn(II) complexes shows that the naphthyl protons close to the metal ion is H(8) rather than H(2) in the $(edta1nap)^{2-}$ complex, and H(3) rather than H(1) in the $(edta2nap)^{2-}$ complex. These structural features are visualized in Fig. 8 with the aid of molecular mechanics $MM^+$ [26]; the rough structural parameters related to the features are given in the caption. In both complexes, naphthalene rings face each other with a close contact, leading to the high efficiencies of excimer formation in the Zn(II) complexes; as a result, the intensity ratios $I_E/I_M$ are much larger than those of the corresponding uncoordinated ligands. The slow geometrical interconversion in [Zn(edta1nap)($H_2O$)] is due to the steric and size effects of naphthyl groups; the 'heavy' aromatic ring retards the conformational rearrangement. This dynamic property is also responsible for the efficiency of excimer formation in the ground sate of the Zn(II) complex.

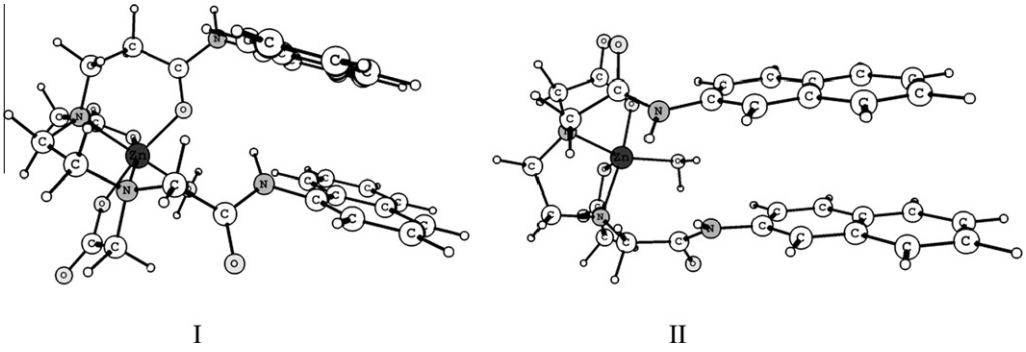

I II

**Fig. 8.** Structural features in (I) [Zn(edta1nap)($H_2O$)] and (II) [Zn(edta2nap)($H_2O$)]; the structures are drawn with the aid of molecular mechanics just to visualize best the structural information obtained by NMR of the Zn and Mn complexes. Interatomic distances (Å) in the view of I: Zn–O(amide), 1.9 and 4.5; Zn–H(8), 4.3 and 4.6; C(5)–C(2′), 3.4. Interatomic distances (Å) in the view of II: Zn-O(amide), 3.9 and 4.0; Zn–H(3), 3.4 and 4.4; C(1)–C(1′), 3.5. The parallel stacks of naphthalene rings with close contacts are responsible for the intense excimer emission of the Zn complexes.

This study presents a rare example of the isomeric ligands that give metal complexes having quite distinct structural properties in solution. The ligands differ only in the substitution position of the naphthalene unit. Moreover, the naphthyl arms do not directly participate in the metal coordination. However, the resulting metal complexes have the striking differences in the structural and dynamic properties, which govern the excimer formation and the emission process.

## Acknowledgements

This work was supported in part by the Consejo Nacional de Ciencia y Tecnología de México (CONACYT, Project No. 79272). The NMR spectrometer is operated under the support of the Secretaría de Educación Publica, México (SES-SEP, programs No. P/PIFI 2008-26 and No. P/FPCU2008-07).

## Appendix

Chemical shifts $\delta_{rc}$ due to the ring current of a naphthalene ring are calculated as the sum of dipole fields induced by two hexagons [21]

$$\delta_{rc} = -27.6 \sum_j (1 - 3\cos^2\theta_j) R_j^{-3} \qquad (12)$$

Here, $R_j$ is a distance (in Å) from the center of hexagon $j$, and $\theta_j$ is the angle between the vector $R_j$ and the normal to the hexagon center. The values of $\delta_{rc}$ are given in Table A1 for a resonant proton located above a selected position of a naphthalene ring at a given distance from the ring plane by assuming regular hexagons with C–C = 1.4 Å and C–H = 1.1 Å.

**Table A1**
Ring-current shift $\delta_{rc}$ of a proton that resides above a selected position of a naphthalene ring at a given height $Z$ (Å) from the ring plane.

| $Z$ | Mol. center | Hex. center | C$\alpha$[a] | C$\beta$[a] | C9,10 | H$\alpha$[a] | H$\beta$[a] |
|---|---|---|---|---|---|---|---|
| 3 | −2.6 | −2.4 | −1.4 | −1.2 | −2.2 | −0.4 | −0.3 |
| 3.5 | −1.8 | −1.7 | −1.1 | −0.9 | −1.6 | −0.5 | −0.4 |
| 4 | −1.3 | −1.2 | −0.8 | −0.7 | −1.2 | −0.4 | −0.3 |
| 4.5 | −1.0 | −0.9 | −0.7 | −0.6 | −0.9 | −0.4 | −0.3 |
| 5 | −0.7 | −0.7 | −0.5 | −0.5 | −0.7 | −0.3 | −0.3 |

[a] $\alpha$ = 1, 4, 5, 8; $\beta$ = 2, 3, 6, 7.

## References

[1] E.A. Chandross, C.J. Dempster, J. Am. Chem. Soc. 92 (1970) 3586–3593.
[2] R.J. Locke, E.C. Lim, J. Phys. Chem. 93 (1989) 6017–6019.
[3] M.T. Albelda, M.A. Bernardo, P. Diaz, E. Garcia-Espana, J.S. de Melo, F. Pina, C. Soriano, V.L.E. Santiago, Chem. Commun. (2001) 1520–1521.
[4] J. Kawakami, A. Fukushi, S. Ito, Chem. Lett. (1999) 955–956.
[5] J. Kawakami, Y. Komai, T. Sumori, A. Fukushi, K. Shimozaki, S. Ito, J. Photochem. Photobiol. A: Chem. 139 (2001) 71–78.
[6] J. Kawakami, T. Niiyama, S. Ito, Anal. Sci. 18 (2002) 735–736.
[7] Y. Suzuki, T. Morozumi, H. Nakamura, M. Shimomura, T. Hayashita, R.A. Bartsh, J. Phys. Chem. B 102 (1998) 7910–7917.
[8] R. Tahara, T. Morozumi, Y. Suzuki, Y. Kakizawa, T. Akita, H. Nakamura, J. Incl. Phenom. Mol. Recog. Chem. 32 (1998) 283–294.
[9] F. Sancenon, A.B. Descalzo, J.M. Lloris, R. Martinez-Manez, T. Pardo, M.J. Segui, J. Soto, Polyhedron 21 (2002) 1397–1404.
[10] L. Machi, H. Santacruz, M. Sanchez, M. Inoue, Supramol. Chem. 18 (2006) 561–569.
[11] L. Machi, H. Santacruz, M. Sanchez, M. Inoue, Inorg. Chem. Commun. 10 (2007) 547–550.
[12] L. Machi, I.C. Munoz, R. Perez-Gonzalez, M. Sanchez, M. Inoue, Supramol. Chem. 21 (2009) 665–673.
[13] M. Inoue, Excel® worksheets for Spectrometry, Universidad de Sonora.
[14] F. Pina, M.A. Bernardo, E. Garcia-Espana, Eur. J. Inorg. Chem. (2000) 2143–2157.
[15] C. Ichimura, Y. Shiraishi, T. Hirai, Tetrahedron 66 (2010) 5594–5601.
[16] R. Aucejo, J. Alarcon, E. Garcia-Espana, J.M. Llinares, K.L. Marchin, C. Soriano, C. Lodeiro, M.A. Bernardo, F. Pina, J. Pina, J.S. de Melo, Eur. J. Inorg. Chem. (2005) 4301–4308.
[17] C. Bazzicalupi, A. Bencini, S. Biagini, E. Faggi, G. Farruggia, G. Andreani, P. Gratteri, L. Prodi, A. Spepia, B. Valtancolia, Dalton Trans. 39 (2010) 7080–7090.
[18] M.B. Inoue, P. Oram, G. Andreuderiquer, M. Inoue, P. Borbat, A. Raitsimring, Q. Fernando, Inorg. Chem. 34 (1995) 3528–3535.
[19] M.B. Inoue, F. Medrano, M. Inoue, A. Raitsimring, Q. Fernando, Inorg. Chem. 36 (1997) 2335–2340.
[20] M.B. Inoue, I.C. Munoz, M. Inoue, Q. Fernando, Inorg. Chim. Acta 300 (2000) 206–211.
[21] J.A. Pople, W.G. Schneider, H.J. Bernstein, High-resolution Nuclear Magnetic Resonance, McGraw-Hill, New York, 1959.
[22] M.B. Inoue, C.A. Villegas, K. Asano, M. Nakamura, M. Inoue, Q. Fernando, Inorg. Chem. 31 (1992) 2480–2483.
[23] M.B. Inoue, R.E. Navarro, M. Inoue, Q. Fernando, Inorg. Chem. 34 (1995) 6074–6079.
[24] A. Carrington, A.D. McLachlan, Introduction to Magnetic Resonance, Harper & Row, New York, 1969.
[25] R.E. Navarro, H. Santacruz, M. Inoue, J. Inorg. Biochem. 99 (2005) 584–588.
[26] Hyper-Chem for Windows, Professional Version-Rel. 6.03, Hypercube Inc., Gainesville, Fl.